Carbon Dioxide Uptake

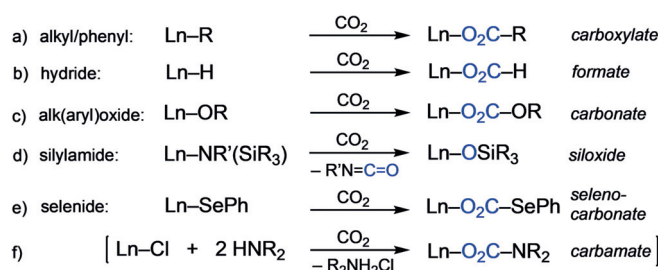# Effective and Reversible Carbon Dioxide Insertion into Cerium Pyrazolates

Uwe Bayer, Daniel Werner, Cäcilia Maichle-Mössmer, and Reiner Anwander*

Abstract: *The homoleptic pyrazolate complexes [Ce$^{III}_4$-(Me$_2$pz)$_{12}$] and [Ce^{IV}(Me$_2$pz)$_4$]$_2$ quantitatively insert CO$_2$ to give [Ce$^{III}_4$(Me$_2$pz·CO$_2$)$_{12}$] and [Ce^{IV}(Me$_2$pz·CO$_2$)$_4$], respectively (Me$_2$pz = 3,5-dimethylpyrazolato). This process is reversible for both complexes, as observed by in situ IR and NMR spectroscopy in solution and by TGA in the solid state. By adjusting the molar ratio, one molecule of CO$_2$ per [Ce^{IV}-(Me$_2$pz)$_4$] complex could be inserted to give trimetallic [Ce$_3$-(Me$_2$pz)$_9$(Me$_2$pz·CO$_2$)$_3$(thf)]. Both the cerous and ceric insertion products catalyze the formation of cyclic carbonates from epoxides and CO$_2$ under mild conditions. In the absence of epoxide, the ceric catalyst is prone to reduction by the co-catalyst tetra-n-butylammonium bromide (TBAB).*

Introduction

Inexorably rising CO$_2$ levels in the earth's atmosphere—and their consequential environmental impact—have spurred much interest in combating CO$_2$ build-up.[1] Capture technologies, such as carbon dioxide capture and storage (CCS) and direct air capture (DAC),[2] and CO$_2$ conversion into fuels or chemical feedstocks[3] appear promising. However, such tactics suffer from either a lack of appropriate storage and transportation of CO$_2$, or overcoming the high activation barrier of CO$_2$.[4] To date, the most effective sorbents for CCS/DAC are alkali-metal/alkaline-earth metal hydroxide solutions, inorganic salts (e.g. alkali-metal carbonates),[1,2] or high-surface supported polyamines (max. CO$_2$ sorption capacity ca. 3 mmol g^{-1} at 1 bar)[5] and magnesium-based metal-organic frameworks (ca. 35 wt% or 8 mmol CO$_2$ g^{-1} at 1 bar).[6]

Like alkaline-earth metals, rare-earth metals (Ln) feature a high affinity for carbon dioxide (cf. bastnaesite is the most important Ln^{III} deposit in the Earth's crust). Thus, metal-organic derivatives easily react with or insert CO$_2$, as initially demonstrated by Bochkarev et al. for homoleptic silylamides

[*] U. Bayer, Dr. D. Werner, Dr. C. Maichle-Mössmer,
Prof. Dr. R. Anwander
Institut für Anorganische Chemie
Eberhard Karls Universität Tübingen
Auf der Morgenstelle 18, 72076 Tübingen (Germany)
E-mail: reiner.anwander@uni-tuebingen.de

Supporting information and the ORCID identification numbers for some of the authors of this article can be found under:
https://doi.org/10.1002/anie.201916483.

Scheme 1. Irreversible reaction of carbon dioxide with archetypal organo-rare-earth-metal complexes, with the exception of (e) as shown for (C$_5$Me$_5$)$_2$Sm(SePh)(thf).[22]

Ln[N(SiMe$_3$)$_2$]$_3$[7,8] and alkoxides [Ln(OnBu)$_3$] (Scheme 1c,d).[9,10]

Similar archetypes (including Ln^{III} aryloxides) can also be used for chemical transformations, such as the catalytic conversion of a CO$_2$/epoxide mixture into cyclic carbonates[11] or copolymers.[10a,12,13] However, highly reactive organo-rare-earth-metal complexes such as alkyl[14] and hydride[10a,15] (Scheme 1a,b) or divalent derivatives[16] display irreversible CO$_2$ insertion or favor additional transformations through CO$_2$ post-activation (e.g. formation of CO, CO$_3^{2-}$, C$_2$O$_4^{2-}$).[16] Recently, cerium, the most abundant rare-earth element, has gained attention for CO$_2$ activation.[8,17–19] For example, while the hydrogen-bonded Ce^{IV} oxo complex [(L$_{OEt}$)$_2$Ce=O-(H$_2$O)]·MeC(O)NH$_2$ (L$_{OEt}^-$ = [Co(η^5-C$_5$H$_5$){P(O)(OEt)$_2$}$_3$]$^-$) was shown to form the tetravalent carbonate species [(L$_{OEt}$)$_2$Ce(CO$_3$)],[17] ortho-NHC-substituted aryloxide Ce^{III} complexes (NHC = N-heterocyclic carbene) insert CO$_2$ into the Ce–C$_{NHC}$ bond in a semireversible manner, and catalytically form propylene carbonate from propylene oxide.[18,19]

Bulky cyclopentadienyl (Cp) derivatives (e.g. Ln-(C$_5$Me$_5$)$_3$) were shown to accommodate CO$_2$ insertion in a unidirectional manner, thereby forming very stable carboxylato moieties through a η^5-to-η^1 switch in the C$_5$Me$_5$ coordination (cf. Scheme 1a).[20] Pyrazolates (pz), on the other hand, are dinitrogen-derived Cp counterparts, where the putative N–CO$_2$ bond may tolerate a more reversible insertion process, as seen for other CO$_2$-heteroatom bonds (Scheme 1e).[21,22] As the tetravalent [Ce(Me$_2$pz)$_4$]$_2$ complex was recently shown to undergo reversible insertion of ketones into the Ce–N bond,[23] we extended the study toward CO$_2$. Quantitative insertion of CO$_2$ into the Ce–N(Me$_2$pz) bond was observed for both tetravalent and trivalent cerium Me$_2$pz complexes, and intriguingly the insertion process was found to be fully reversible.

Results and Discussion

Carbon Dioxide Insertion into a Ceric Pyrazolate: Treatment of $[Ce(Me_2pz)_4]_2$ (**1**) with excess CO_2 in either toluene or thf (under 1 bar CO_2 pressure) led to a color change from dark red to orange within 5 minutes (Scheme 2). Crystallization from concentrated toluene or thf solutions at $-40\,°C$ gave orange crystals of $[Ce(Me_2pz \cdot CO_2)_4]$ with either toluene (**2·toluene**, 54%) or thf (**2·thf**, 64%) within the lattice. Discounting the lattice solvent, this accounts for about 25 wt% CO_2 or 5.7 mmol CO_2 per gram.
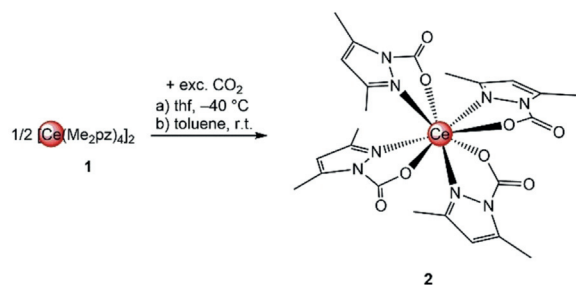
Scheme 2. Insertion of CO_2 into the Ce−N(Me₂pz) bond of [Ce-(Me₂pz)₄]₂ at: a) $-40\,°C$ in thf or b) ambient temperature in toluene.

The molecular structure of **2·toluene** revealed an 8-coordinate cerium(IV) center with four $\kappa^2(N,O)$-coordinating $Me_2pz \cdot CO_2$ ligands (Figure 1), in contrast to the $\kappa^2(O,O)$ modes in carboxylates and related carbamates. The Ce−N and Ce−O bond lengths average 2.528 Å and 2.255 Å, respectively, thus matching the values found in the benzophenone-inserted product $[Ce(Me_2pz)_2(pdpm)_2]$ (Ce1−N1 2.564 Å, Ce1−O1 2.173 Å; pdpm = (3,5-dimethylpyrazol-1-yl)diphenylmethanolate).[23] Other homoleptic Ce^{IV} complexes, [Ce-(L)₄] (with L as a donor-functionalized alkoxy ligand engaged in a 5-membered chelate to cerium), also have similar Ce−O bond lengths as those in **2**, thus highlighting a common chelating coordination motif.[24,25] Seemingly, no delocalization occurs across the O=C−O fragment, which exhibits average C−O bond lengths of 1.207 Å (terminal) and 1.291 Å (bridging). Support for the localization of the C−O double bond came from DRIFTS measurements of **2·toluene** and
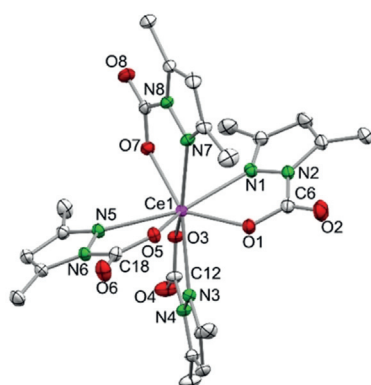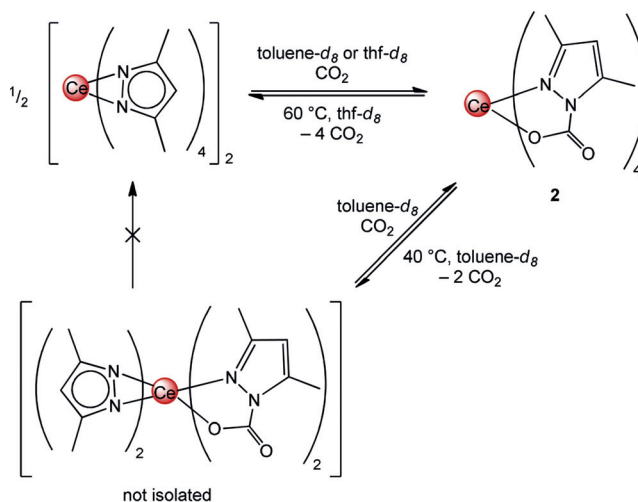
2·thf, which showed the presence of a strong absorption band at $\tilde{\nu} = 1732$ and $1718\ cm^{-1}$, respectively, for the CO stretching of the C−O double bond as well as a strong absorption band at $\tilde{\nu} = 1336\ cm^{-1}$ for the CO stretching of the C−O single bond.

The structure was also supported by NMR spectroscopic measurements. The ^1H NMR spectrum recorded in $[D_8]$toluene at ambient temperature revealed two distinct methyl group environments for all the pyrazolato ligands, indicative of ligand asymmetry and complete consumption of $[Ce(Me_2pz)_4]_2$. The ^{13}C signal of the inserted CO_2 was detected at $\delta = 149.9$ ppm, a region where pyrazolate N-CO_2R signals are expected.[26] ^1H NMR measurements on **2·thf** in $[D_8]$THF at ambient temperature showed a mixture of products, which could not be assigned. Cooling the solution to $-40\,°C$ under 1 bar CO_2 pressure led to a color change from red to orange and both the ^1H and ^{13}C NMR spectra recorded at $-40\,°C$ showed similar signals as **2·toluene** in $[D_8]$toluene.

Variable-temperature (VT) NMR studies of **2·toluene** and **2·thf** in $[D_8]$toluene and $[D_8]$THF were conducted to investigate the reversibility of CO_2 insertion (Scheme 3). In $[D_8]$toluene, the formation of a new species at $40\,°C$ was revealed and no further liberation of CO_2 was observed even after heating above $60\,°C$ (see Figure S6 in the Supporting Information). The ^1H NMR spectrum recorded at $40\,°C$ shows two sets of signals for different Me₂pz moieties in a 1:1 ratio, which suggests the formation of putative compound $[Ce-(Me_2pz)_2(Me_2pz \cdot CO_2)_2]$.

Recooling the solution did not reform **2·toluene** quantitatively, likely because some of the liberated CO_2 was no longer within the reaction medium, but the addition of fresh CO_2 quantitatively reformed **2·toluene**. The $[D_8]$THF VT NMR experiment of compound **2·thf** showed a different CO_2-deinsertion behavior (see Figure S10). As a consequence of competitive thf coordination, displacement of CO_2 starts at $10\,°C$ and is complete at $60\,°C$, with formation of $[Ce(Me_2pz)_4\text{-}(thf)]$. As seen in the experiment in $[D_8]$toluene, this reaction is fully reversible by recooling the sample and subsequently

Figure 1. Crystal structure of $[Ce(Me_2pz \cdot CO_2)_4]$ (**2·toluene**). Ellipsoids are shown at the 50% probability level. Hydrogen atoms and lattice toluene are omitted for clarity. Selected bond lengths/angles are listed in the Supporting Information.

Scheme 3. Reversible insertion of CO_2 into the Ce−N(Me₂pz) bond. The process is completely reversible in $[D_8]$thf and partially reversible in $[D_8]$toluene. The product arising from the elimination of CO_2 in $[D_8]$toluene has not been isolated; the structure is based on ^1H NMR spectroscopic analysis at $40\,°C$.
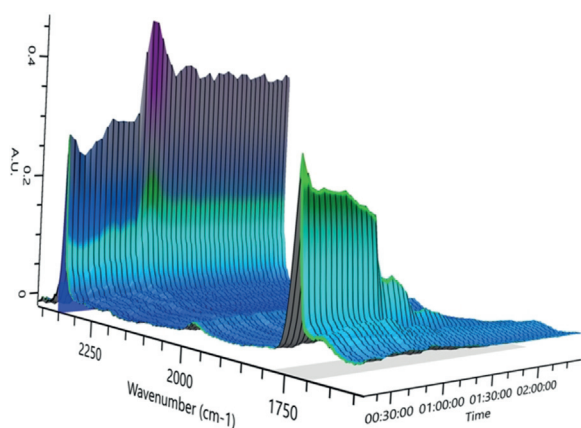
Figure 2. In situ IR spectroscopy of **2·thf** at 60 °C in the range of $\tilde{\nu} = 1700$ to $2350 \ cm^{-1}$. Normalized intensities are shown. Spectra were recorded every minute.

Scheme 4. Insertion of one equivalent of CO_2 into the Ce–N(Me$_2$pz) bond of [Ce(Me$_2$pz)$_4$(thf)].

introducing CO_2. Additionally, in situ IR measurements were performed at 60 °C, which showed complete loss of inserted CO_2 and formation of free CO_2 (Figure 2 and see also Figure S58).

In the solid state, **2·toluene** is stable for several weeks at −40 °C, but at ambient temperature it partially loses CO_2 over a few days or when it is exposed to vacuum, as indicated by a color change from orange to dark red. A thermogravimetric analysis (TGA), performed under a flow of Ar and heating the sample slowly from 28 °C to 250 °C, indicated an initial loss of mostly lattice toluene. The liberation of CO_2 and small amounts of lattice toluene was dominant between 55 and 95 °C, as revealed by a step of 21.92 % (theoretical proportion of CO_2 in **2·toluene** 19.98 %). At 250 °C, only nonvolatile parts of **2·toluene** remain, leaving a mass of 49.79 % of the initial weight (theoretical value 51.61 %; see Figure S59). Although the deinsertion of carbon dioxide was achieved in the solid state, bulk compound **1** did not insert any carbon dioxide when stored under 1 bar CO_2 pressure for three days. Moreover, compound **1** was hydrolyzed upon exposure to air within one hour (DRIFT spectrum, see Figure S57).

[Ce(Me$_2$pz)$_4$(thf)] (**1·thf**) was treated with stoichiometric amounts of CO_2 to generate the putative [Ce-(Me$_2$pz)$_2$(Me$_2$pz·CO_2)$_2$] (Scheme 3). Although this species could not be isolated, it was possible to generate mono-inserted [Ce$_3$(Me$_2$pz)$_9$(Me$_2$pz·CO_2)$_3$(thf)] (**3**) in moderate yields of 46 % (Scheme 4). The crystal structure of ceric **3** shows a ring motif with two distinct 9-coordinate and one 10-coordinate cerium atoms (Figure 3). Although all the cerium centers are coordinated by three Me$_2$pz ligands in an $\eta^2(N,N')$ fashion, Ce1 connects further to two oxygen atoms of neighboring Me$_2$pz·CO_2 ligands as well as an additional thf molecule, 10-coordinate Ce2 is surrounded by two κ^2:(N,O)-chelating Me$_2$pz·CO_2 ligands, and Ce3 exhibits additional contacts to one κ^2:(N,O)-Me$_2$pz·CO_2 ligand and an oxygen atom of a neighboring Me$_2$pz·CO_2 ligand.

Each Me$_2$pz·CO_2 ligand bridges between two cerium atoms. In contrast to homoleptic **2**, all the oxygen atoms are engaged in cerium bonding, which implies delocalized O–C–O bonds (av. C–O, 1.247 Å). The $\eta^2(N,N')$-Ce–N(Me$_2$pz)
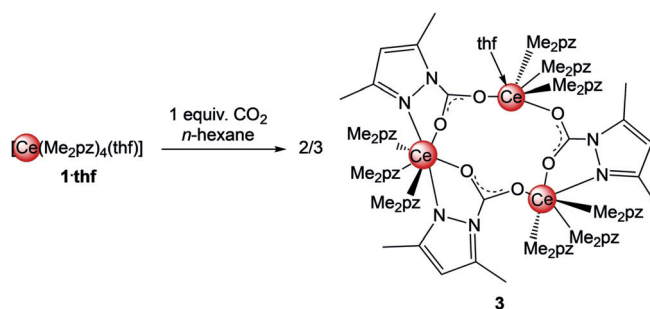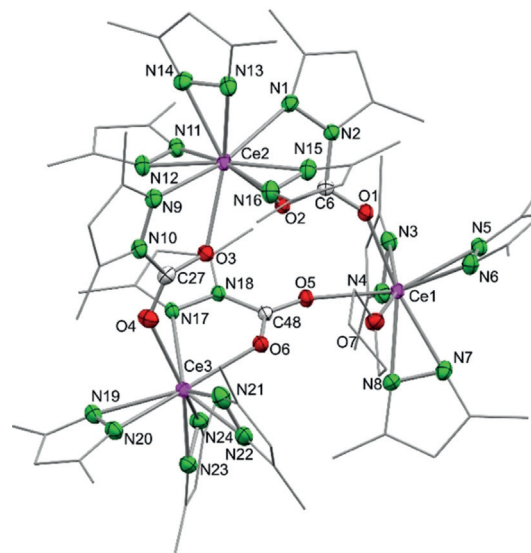
Figure 3. Crystal structure of [Ce$_3$(Me$_2$pz)$_9$(Me$_2$pz·CO_2)$_3$(thf)] (**3**). Ellipsoids are shown at the 50 % probability level. Hydrogen atoms and lattice *n*-hexane are omitted for clarity. Selected bond lengths/angles are listed in the Supporting Information.

bond lengths are in the expected range.[24,27] According to VT NMR studies carried out in [D$_8$]toluene, the trimetallic entity **3** is retained in solution at low temperatures, with every dimethylpyrazolato ligand showing a distinct signal set in the proton NMR spectrum at −80 °C (see Figure S12). The signals for the protons of the bridging Me$_2$pz·CO_2 ligands are shifted upfield compared to those of the terminal $\eta^2(N,N')$-Me$_2$pz ligands. As a consequence of the equilibrium between potential alternative oligomers formed in the presence of only one equivalent of CO_2 per cerium, the interpretation of the ambient-temperature NMR spectrum was difficult. This was already experienced for the insertion of benzophenone into the Ce–N(Me$_2$pz) bond.[23] Upon heating to 90 °C, CO_2 was liberated and [Ce(Me$_2$pz)$_4$] re-formed (see Figure S14). After cooling to ambient temperature, a partial reinsertion of CO_2 was observed, as was found in the VT NMR experiments on **2·toluene** and **2·thf**.

Carbon Dioxide Insertion into a Cerous Pyrazolate: To examine the role of the oxidation state of cerium (Ce^{IV} versus Ce^{III}) and, therefore, the impact of its Lewis acidity, cerous donor-free [Ce$_4$(Me$_2$pz)$_{12}$][28] (**4**) was used as a precursor for CO_2 insertion (Scheme 5). Remarkably, while retaining the

Ce_4 nuclearity, all of the $Ce-N(Me_2pz)$ moieties engaged in CO_2 insertion, leading to the complex $[Ce_4(Me_2pz \cdot CO_2)_{12}]$ (**5**; Figure 4). Compared to the six different coordination modes of the pyrazolato moieties in starting material **4**,[28] the crystal structure of **5** revealed only three. Ce2, Ce3, and Ce4 form a nearly equilateral triangle bridged by μ_3-$1\kappa^2(N,O):2\kappa(O):3\kappa$-$(O')$-$Me_2pz \cdot CO_2$. Each of the 9-coordinate cerium centers (Ce2, Ce3, and Ce4) is also surrounded by two terminal $Me_2pz \cdot CO_2$ groups in a $\kappa^2(N,O)$ coordination mode and two oxygen atoms in a $\kappa^2(O,O')$ fashion (Figure S66). This triangle is capped by 9-coordinate Ce1, which is coordinated to three $Me_2pz \cdot CO_2$ ligands in a $\kappa^2(N,O)$ manner ($Ce1-N_{avg}$ 2.710 Å, $Ce1-O_{avg}$ 2.395 Å) and to three bridging oxygen atoms. The $Ce-O$ bond lengths are similar to those found in $[Ce(L^R \cdot CO_2)_3]$ ($L^R = 2$-O-$3,5$-tBu_2-$C_6H_2(1$-$C\{N(CH)_2N(R)\})$) and $R = iPr$ and Mes) reported by Arnold et al. with $Ce-O$ bond lengths of 2.466(6)–2.482(6) Å.[18b] The $O-C-O$ bond lengths

indicate delocalization of the bridging $Me_2pz \cdot CO_2$ ligands, with two $C-O$ bond lengths in the same region (1.235(9)–1.264(9) Å) and rather localized $C-O$ single (1.26(1)–1.301(9) Å) and $C-O$ double bonds (1.21(1)–1.229(9) Å) for the capping and terminal $Me_2pz \cdot CO_2$ ligands. For further comparison, the cerous carbamate $[Ce_4(O_2CNiPr_2)_{12}]$ features a lozenged arrangement of one 8-coordinate and three 7-coordinate Ce^{III} centers with $Ce-O$ bond lengths in the range 2.322(7)–2.746(7) Å (no Ce-N interaction).[29] The latter complex was obtained from the reaction of $CeCl_3(DME)$ with $HNiPr_2$ and CO_2 (Scheme 1f). In accordance with the crystal structure of cluster **5**, DRIFTS measurements show strong absorption bands for both the $C-O$ single bonds ($\tilde{v} = 1250$–1350 cm^{-1}) and $C-O$ double bonds ($\tilde{v} = 1600$–1750 cm^{-1}). ^{1}H DOSY NMR measurements on **5** in $[D_8]$toluene, $[D_8]$THF, or a $[D_8]$toluene/3,3-dimethyl-1,2-butylene oxide mixture revealed distinct diffusion coefficients (see Figures S17–S20) for the solvents employed and only one additional peak corresponding to a much larger species but correlating with every other signal in the proton NMR spectra. Calculation of the molar mass of this compound ($[D_8]$toluene: $M_r = 1989$ g mol^{-1}; $[D_8]$THF: $M_r = 1643$ g mol^{-1}; $[D_8]$toluene + 3,3-dimethyl-1,2-butyleneoxide: $M_r = 2357$ g mol^{-1}) as a compact sphere-like molecule[30] suggests it exists as a tetrametallic ($M_r = 2242$ g mol^{-1}) or a non-monometallic species in solution. Treating $[Ce(Me_2pz)_3(thf)]_2$ with CO_2 in $[D_8]$THF gave the same NMR spectrum as that of **5·toluene**, thus indicating the formation of a multimetallic compound also in donor solvents (see Figure S16). TGA of **5·toluene** also showed an initial loss of toluene (cf. **2·toluene**), followed by a pronounced step (21.39% weight loss) in the range from 52 to 90 °C, consistent with the release of CO_2 (theoretical value: 16.75%) and some lattice toluene (Figure S60). At 250 °C, only the nonvolatile parts of **5·toluene** remain and a total loss of 46.82 wt% compared to the starting material fits well with the theoretical value of 45.99% for 10 molecules of toluene and 12 molecules of CO_2 eliminated from $[Ce_4(Me_2pz \cdot CO_2)_{12}] \cdot 10$ toluene (**5·toluene**).
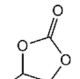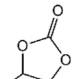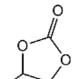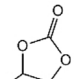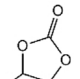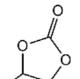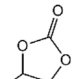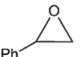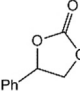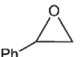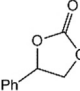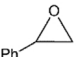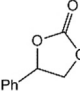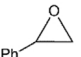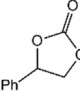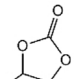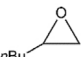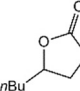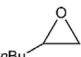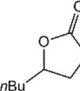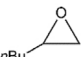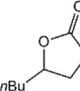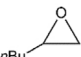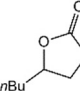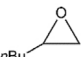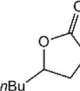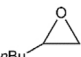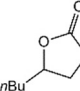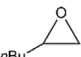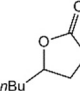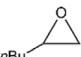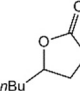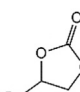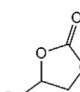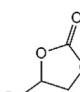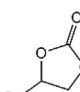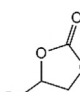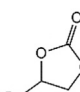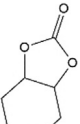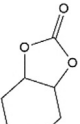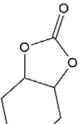
Catalytic Formation of Cyclic Carbonates from CO_2 and Oxiranes: Having established the efficiency and reversibility of CO_2 insertion into $Ce-N(Me_2pz)$ bonds, we were interested in any catalytic utilization. Accordingly, pyrazolate complexes **1** and **4** were probed as catalysts for the generation of cyclic carbonates from CO_2 and oxiranes. In the absence of CO_2, compound **1** interacts with epoxides, as indicated by a noticeable shift in the ^{1}H NMR spectrum upon addition of one equivalent of 3,3-dimethyl-1,2-butylene oxide (see Figure S24). This is most likely due to formation of a donor adduct, which is considered a crucial step in Lewis-acid-catalyzed cycloaddition reactions. Even though such donor adducts were shown to be isolable (e.g. $Tp^{tBu}Ca(O$-$2,6$-$iPr_2C_6H_3) \cdot (PO)$; $Tp^{tBu} = tris(3$-tBu-pyrazolyl)borato, $PO = $ propylene oxide[31]), the putative $[Ce(Me_2pz)_4(PO)]$ (**1-PO**) could not be isolated. Tetra-n-butylammonium bromide (TBAB) was employed as a co-catalyst, since it was shown to promote the highest activities in such cycloaddition reactions.[11b,32] The reaction was optimized for propylene oxide, which gave almost quantitative conversion after 24 h under mild conditions. Using 0.5 mol% **1** or 0.25 mol% **4** and

Scheme 5. Insertion of of CO_2 into the $Ce-N(Me_2pz)$ bonds of cerous $[Ce_4(Me_2pz)_{12}]$.

Figure 4. Crystal structure of $[Ce_4(Me_2pz \cdot CO_2)_{12}]$ (**5**). Ellipsoids are shown at the 50% probability level. Hydrogen atoms and lattice toluene (ten molecules) are omitted for clarity. Cutouts of the crystal structure of **5** and a schematic view of different $Me_2Pz \cdot CO_2$ binding modes, as well as selected bond lengths/angles are shown in the Supporting Information.

1 mol% TBAB without solvent at ambient temperature and 1 bar CO_2 pressure gave 93% conversion for the tetravalent catalyst **1** and 98% for its trivalent counterpart (Table 1, entries 1 and 3). The CO_2-insertion complexes **2** and **5** displayed similar catalytic activity (entries 2 and 4). The conversion dropped drastically on increasing the steric bulk of the substituent on the epoxides. As a result, styrene oxide, and 3,3-dimethyl-1,2-butylene oxide showed only very low conversions (entry 21) for ceric **1** and almost no conversion in the case of trivalent catalyst **4** (entry 22). Moderate conversion was observed for 1,2-*n*-hexylene oxide with the tetravalent catalyst **1** (entry 13). Conducting the catalysis at higher

Table 1: Catalytic formation of cyclic carbonates from epoxides and CO_2.[a]

Entry	Catalyst	Substrate	Product	Conversion [%]	TON/Ce
1	**1**			93	93
2	**2**			93	93
3	**4**			98	98
4	**5**			96	96
5	**1**[i]			98	196
6	**1**			20	20
7	**1**[b]			4	8
8	**4**			13	13
9	**4**[c]	Ph		6	12
10	**4·thf**		Ph	13	13
11	**4·thf**[c]			7	14
12	**1**[i]			12	24
13	**1**			61	61
14	**4**			25	25
15	**1**[d]			98	98
16	**4**[e]			96	96
17	**1**[f]	*n*Bu		25	25
18	**1**[g]		*n*Bu	76	76
19	**6**			3	3
20	**1**[i]			49	98
21	**1**			12	12
22	**4**			3	3
23	**1**[g]			9	9
24	**1**[h]			84	168
25	**1**[i]	*t*Bu	*t*Bu	14	28
26	**1**[j]			60	300
27	**1**			2	2
28	**1**[h]			77	154
29	**1**[j]			35	175

[a] Reaction conditions if not otherwise noted: 1 bar CO_2 pressure and 0.5 mol% catalyst (1 mol% for **2** and **6**; 0.25 mol% for **4** and **5**) and 1 mol% co-catalyst for 24 h at ambient temperature in neat epoxide. [b] 0.25 mol% catalyst **1** and 0.5 mol% TBAB, 24 h. [c] 0.125 mol% catalyst **4** and 0.5 mol% TBAB, 24 h. [d] 0.5 mol% catalyst **1** and 1 mol% TBAB, 24 h, 90°C. [e] 0.25 mol% catalyst **4** and 1 mol% TBAB, 24 h, 90°C. [f] At 90°C without TBAB as a co-catalyst. [g] 0.5 mol% catalyst **1** and 1 mol% TBAB, 24 h, 10 bar CO_2 pressure. [h] 0.25 mol% catalyst **1** and 0.5 mol% TBAB, 24 h, 90°C, 10 bar CO_2 pressure. [i] 0.25 mol% catalyst **1** and 0.5 mol% TBAB, 1 h, 90°C, 10 bar CO_2 pressure. [j] 0.1 mol% catalyst **1** and 0.2 mol% TBAB, 24 h, 90°C, 10 bar CO_2 pressure.

temperature increased the TONs with both catalysts **1** and **4**, and resulted in nearly quantitative conversion for both systems (entries 15 and 16). Without co-catalyst TBAB, **1** showed moderate catalytic activity at 90°C (entry 17). In almost all cases, tetravalent **1** showed higher catalytic activity than cerous **4**, which most likely results from the higher Lewis acidity of Ce^{IV} versus Ce^{III}. To further evaluate the catalytic reaction with catalyst **1** and propylene oxide, the TOFs at different stages of the catalysis were determined (see Table S1). After a short induction period, most likely corresponding to the insertion of CO_2 into **1**, the TOF reached a maximum of 11 h^{-1} within the first 3 h. For comparison, a TOF of 155 h^{-1} was reported by Yao and co-workers when performing the reaction under 10 bar CO_2 pressure.[11a] Increasing the CO_2 pressure did not significantly affect the catalytic activity of compound **1** (entries 13 vs. 18 and 21 vs. 23). However, a simultaneous increase of the temperature to 90°C and the CO_2 pressure to 10 bar led to a marked improvement in the catalytic activity, resulting in TONs of up to 300 for the sterically demanding 3,3-dimethyl-1,2-butylene oxide (entries 24 and 26). The latter conditions were also applicable for the cycloaddition of CO_2 and cyclohexene oxide, an internal epoxide (entries 27–29). Having optimized the reaction conditions, we determined the initial turnover frequencies for the different epoxides (entries 5, 12, 20, and 25). As expected, the TOFs increased as the steric of the substituents bulk decreased, ranging from 24 to 196 h^{-1} and giving almost quantitative conversion of propylene oxide after a reaction time of one hour (entry 5). Compared to the other catalyst systems based on rare-earth metals reported by Yao and co-workers (TOFs up to 440 h^{-1}) or by Otero and co-workers (3167 h^{-1}), our system shows only moderate catalytic activity under comparable conditions.[11a,b]

The mechanism of the cycloaddition of CO_2 and epoxides using tetraalkylammonium salts as co-catalysts has been discussed in detail.[32,33] It is generally accepted that the epoxide is activated by coordination to a Lewis-acidic metal center followed by a nucleophilic ring-opening attack of the bromide to form a metal-alkoxy bond (Scheme 6). Subsequently, the alkoxide reacts with CO_2 and cyclizes to produce a cyclic carbonate. Hints that the mechanisms for the cycloaddition differ using ceric **1** or cerous **4** as the catalyst could be found when conducting the reactions with different amounts of catalyst loading (entries 7 and 9). This results in a change in the TONs for the tetravalent catalyst **1**, whereas the TONs remained the same for trivalent complex **4**. The occurrence of distinct reaction mechanisms is not surprising, as **1** is a monometallic complex while **4** is a tetrametallic compound in the solid state and in solution (for a more detailed possible mechanism see Scheme S1). Such a mechanism, involving multiple metal centers, was previously proposed for the bimetallic complex $[Al(salen)]_2O$ by North and co-workers.[32] However, any detailed information about the mechanism could not be retrieved from our catalyst system as the TOFs decreased enormously when the reactions were conducted in propylene carbonate (no significant conversion at ambient temperature after 24 h and ca. 10% conversion after 20 h at 90°C) or any other solvent, which makes kinetic studies unfeasible.
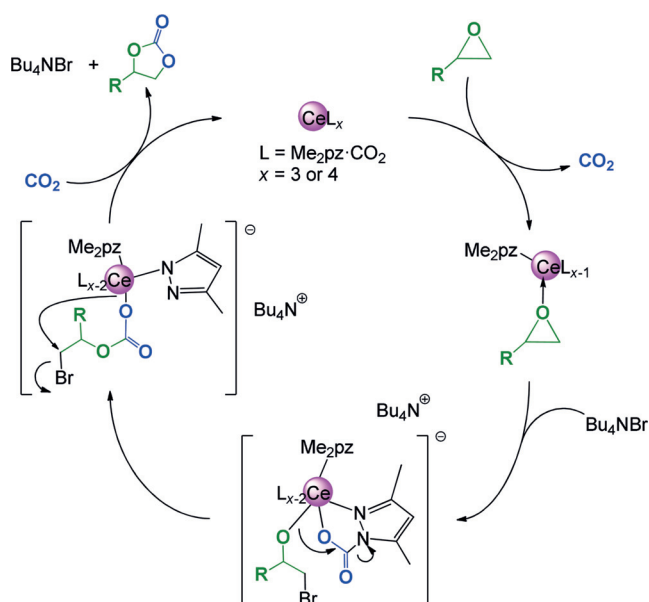
Scheme 6. Proposed overall mechanism for the coupling of CO_2 with epoxides.

dioxide with TBAB as a co-catalyst under mild conditions. We are currently investigating the carbon dioxide capture performance of silica-grafted variants of Ce-pyrazolates,[34] and our findings might also stimulate research in the area of cerium-dipyrazolate-based CO_2-"breathable"/expandable MOFs.[35,36]

Conflict of interest

The authors declare no conflict of interest.

Complex **2** underwent a reductive side reaction in the presence of TBAB to afford cerous species [Ce(Me$_2$pz·CO$_2$)$_4$][NBu$_4$] (**6**). This side reaction occurred during the catalytic studies and when combining **1** and TBAB in stoichiometric amounts in [D$_8$]toluene under 1 bar CO_2 pressure. Although **2** is very stable in toluene solution under these conditions (no color change was observed after several days), it underwent reduction in the presence of TBAB within hours, as evidenced by decolorization of the orange solution. Most probably bromine is formed as an oxidation product; however, no brominated product could be detected in the reaction mixture (see Figure S23). The use of epoxides as a solvent seems to stabilize the tetravalent **2**, as no paramagnetic signals were found in the ^{1}H NMR spectra of the catalytic reactions. The crystal structure of **6** revealed the same motif as seen in **2·toluene** and **2·thf** (see Figure S67). The 8-coordinate cerium center bears four $\kappa^2(N,O)$ Me$_2$pz·CO$_2$ ligands with elongated Ce–N and Ce–O bonds compared to ceric **2·toluene** and **2·thf**, as would be expected for a cerium(III) center. Cerous **6** displays poor catalytic activity compared to tetravalent **1** (Table 1, entry 19), thus underlining that it is a side product and not the active catalyst.

Conclusion

We have shown that carbon dioxide easily inserts into the Ce–N(Me$_2$pz) bond of both ceric [Ce(Me$_2$pz)$_4$]$_2$ and cerous [Ce$_4$(Me$_2$pz)$_{12}$] at an amount equivalent to 5.7 mmol CO_2 per gram complex and via the controlled activation of 12 molecules of CO_2 within one complex, respectively. The insertion process is reversible both in solution and in the solid state, with CO_2 desorption being complete at < 100 °C. Both trivalent and tetravalent cerium pyrazolate complexes are active catalysts for the cycloaddition of epoxides and carbon

[1] a) P. Falkowski et al., *Science* **2000**, *290*, 291–296; b) S. Solomon, G.-K. Plattner, R. Knutti, P. Friedlingstein, *Proc. Natl. Acad. Sci. USA* **2009**, *106*, 1704–1709; c) R. S. Haszeldine, *Science* **2009**, *325*, 1647–1652; d) D. W. Keith, *Science* **2009**, *325*, 1654–1655; e) N. von der Assen, P. Voll, M. Peters, A. Bardow, *Chem. Soc. Rev.* **2014**, *43*, 7982–7994.

[2] For review articles, see a) D. M. D'Alessandro, B. Smit, J. R. Long, *Angew. Chem. Int. Ed.* **2010**, *49*, 6058–6082; *Angew. Chem.* **2010**, *122*, 6194–6219; b) C.-H. Yu, C.-H. Huang, C.-S. Tan, *Aerosol Air Qual. Res.* **2012**, *12*, 745–769; c) K. Sumida, D. L. Rogow, J. A. Mason, T. M. McDonald, E. D. Bloch, Z. R. Herm, T.-H. Bae, J. R. Long, *Chem. Rev.* **2012**, *112*, 724–781; d) E. S. Sanz-Pérez, C. R. Murdock, S. A. Didas, C. W. Jones, *Chem. Rev.* **2016**, *116*, 11840–11876; e) Y. Lin, C. Kong, Q. Zhang, L. Chen, *Adv. Energy Mater.* **2017**, *7*, 1601296.

[3] For review articles, see a) T. Sakakura, J.-C. Choi, H. Yasuda, *Chem. Rev.* **2007**, *107*, 2365–2387; b) G. Centi, S. Perathoner, *Catal. Today* **2009**, *148*, 191–205; c) M. Cokoja, C. Bruckmeier, B. Rieger, W. A. Herrmann, F. E. Kühn, *Angew. Chem. Int. Ed.* **2011**, *50*, 8510–8537; *Angew. Chem.* **2011**, *123*, 8662–8690; d) M. Aresta, A. Dibenedetto, A. Angelini, *Chem. Rev.* **2014**, *114*, 1709–1742; e) Q. Liu, L. Wu, R. Jackstell, M. Beller, *Nat. Commun.* **2015**, *6*, 5933; f) J. Artz, T. E. Müller, K. Thenert, J. Kleinekorte, R. Meys, A. Sternberg, A. Bardow, W. Leitner, *Chem. Rev.* **2018**, *118*, 434–504.

[4] A. Paparo, J. Okuda, *Coord. Chem. Rev.* **2017**, *334*, 136–149.

[5] a) A. Goeppert, M. Czaun, R. B. May, G. K. S. Prakash, G. A. Olah, S. R. Narayanan, *J. Am. Chem. Soc.* **2011**, *133*, 20164–20167; b) F. Inagaki, C. Matsumoto, T. Iwata, C. Mukai, *J. Am. Chem. Soc.* **2017**, *139*, 4639–4642.

[6] a) S. R. Caskey, A. G. Wong-Foy, A. J. Matzger, *J. Am. Chem. Soc.* **2008**, *130*, 10870–10871; b) T. M. McDonald et al., *Nature* **2015**, *519*, 303–308.

[7] Y. F. Radkov, E. A. Fedorova, S. Y. Khorshev, G. S. Kalinina, M. N. Bochkarev, G. A. Razuvaev, *Zhur. Obshchei Khimii* **1986**, *56*, 386–389.

[8] For a recent study on Ce^{III} silylamides, see H. Yin, P. J. Carroll, E. J. Schelter, *Chem. Commun.* **2016**, *52*, 9813 – 9816.

[9] M. N. Bochkarev, E. A. Fedorova, Y. F. Radkov, S. Y. Khorshev, G. S. Kalinina, G. A. Razuvaev, *J. Organomet. Chem.* **1983**, *258*, C29 – C33.

[10] For examples of CO_2 insertion into Ln^{III}−aryloxy bonds, see a) D. Cui, M. Nishiura, O. Tardif, Z. Hou, *Organometallics* **2008**, *27*, 2428 – 2435; b) L. A. M. Steele, T. J. Boyle, R. A. Kemp, C. Moore, *Polyhedron* **2012**, *42*, 258 – 264.

[11] a) J. Qin, P. Wang, Q. Li, Y. Zhang, D. Yuan, Y. Yao, *Chem. Commun.* **2014**, *50*, 10952 – 10955; b) J. Martínez, J. Fernández-Baeza, L. F. Sánchez-Barba, J. A. Castro-Osma, A. Lara-Sánchez, A. Otero, *ChemSusChem* **2017**, *10*, 2886 – 2890; c) Z. Zhao, J. Qin, C. Zhang, Y. Wang, D. Yuan, Y. Yao, *Inorg. Chem.* **2017**, *56*, 4568 – 4575.

[12] a) D. Cui, M. Nishiura, Z. Hou, *Macromolecules* **2005**, *38*, 4089 – 4095; b) D. V. Vitanova, F. Hampel, K. C. Hultzsch, *J. Organomet. Chem.* **2005**, *690*, 5182 – 5197; c) B. B. Lazarov, F. Hampel, K. C. Hultzsch, *Z. Anorg. Allg. Chem.* **2007**, *633*, 2367 – 2373; d) Z. Zhang, D. Cui, X. Liu, *J. Polym. Sci. Part A* **2008**, *46*, 6810 – 6818; e) A. Decortes, R. M. Haak, C. Martín, M. M. Belmonte, E. Martin, J. Benet-Buchholz, A. W. Kleij, *Macromolecules* **2015**, *48*, 8197 – 8207; f) J. Qin, B. Xu, Y. Zhang, D. Yuan, Y. Yao, *Green Chem.* **2016**, *18*, 4270 – 4275.

[13] For the use of organoscandium(III) complexes in the catalytic hydrosilylation of CO_2, see a) A. Berkefeld, W. E. Piers, M. Parvez, L. Castro, L. Maron, O. Eisenstein, *Chem. Sci.* **2013**, *4*, 2152 – 2162; b) F. A. LeBlanc, W. E. Piers, M. Parvez, *Angew. Chem. Int. Ed.* **2014**, *53*, 789 – 792; *Angew. Chem.* **2014**, *126*, 808 – 811.

[14] a) M. A. St. Clair, B. D. Santarsiero, *Acta Crystallogr. Sect. C* **1989**, *45*, 850 – 852; b) H. Schumann, J. A. Meese-Marktscheffel, A. Dietrich, F. H. Görlitz, *J. Organomet. Chem.* **1992**, *430*, 299 – 315; c) W. J. Evans, C. A. Seibel, J. W. Ziller, R. J. Doedens, *Organometallics* **1998**, *17*, 2103 – 2112; d) F. A. LeBlanc, A. Berkefeld, W. E. Piers, M. Parvez, *Organometallics* **2012**, *31*, 810 – 818.

[15] a) O. T. Summerscales, C. M. Moore, B. L. Scott, M. P. Wilkerson, A. D. Sutton, *Organometallics* **2017**, *36*, 4682 – 4685; b) D. W. Beh, W. E. Piers, I. del Rosar, L. Maron, B. S. Gelfand, C. Gendy, J.-B. Lin, *Dalton Trans.* **2018**, *47*, 13680 – 13688.

[16] a) W. J. Evans, C. A. Seibel, J. W. Ziller, *Inorg. Chem.* **1998**, *37*, 770 – 776; b) W. J. Evans, J. M. Perotti, J. C. Brady, J. W. Ziller, *J. Am. Chem. Soc.* **2003**, *125*, 5204 – 5212; c) N. W. Davies, A. S. P. Frey, M. G. Gardinier, J. Wang, *Chem. Commun.* **2006**, 4853 – 4855; d) J. Andrez, J. Pécaut, P.-A. Bayle, M. Mazzanti, *Angew. Chem. Int. Ed.* **2014**, *53*, 10448 – 10452; *Angew. Chem.* **2014**, *126*, 10616 – 10620; e) M. Xémard, V. Goudy, A. Braun, M. Tricoire, M. Cordier, L. Ricard, L. Castro, E. Louyriac, C. E. Kefalidis, C. Clavaguéra, L. Maron, G. Nocton, *Organometallics* **2017**, *36*, 4660 – 4668; f) A. R. Willauer, D. Toniolo, F. Fadaei-Tirani, Y. Yang, M. Laurent, M. Mazzanti, *Dalton Trans.* **2019**, *48*, 6100 – 6110.

[17] a) Y.-M. So, G.-C. Wang, Y. Li, H. H. Y. Sung, I. D. Williams, Z. Lin, W.-H. Leung, *Angew. Chem. Int. Ed.* **2014**, *53*, 1626 – 1629; *Angew. Chem.* **2014**, *126*, 1652 – 1655; b) G.-C. Wang, Y.-M. So, Y. Li, K.-L. Wong, K.-C. Au-Yeung, H. H. Y. Sung, I. D. Williams, W.-H. Leung, *Chem. Eur. J.* **2015**, *21*, 16126 – 16135.

[18] a) P. L. Arnold, Z. R. Turner, A. I. Germeroth, I. J. Casely, G. S. Nichol, R. Bellabarba, R. P. Tooze, *Dalton Trans.* **2013**, *42*, 1333 – 1337; b) P. L. Arnold, R. W. F. Kerr, C. Weetman, S. R. Docherty, J. Rieb, F. L. Cruickshank, K. Wang, C. Jandl, M. W. McMullon, A. Pöthig, et al., *Chem. Sci.* **2018**, *9*, 8035 – 8045.

[19] For further examples of CO_2 insertion into Ln−NHC bonds, see a) P. L. Arnold, I. A. Marr, S. Zlatogorsky, R. Bellabarba, R. P. Tooze, *Dalton Trans.* **2014**, *43*, 34 – 37; b) T. Simler, T. J. Feuerstein, R. Yadav, M. T. Gamer, P. W. Roesky, *Chem. Commun.* **2019**, *55*, 222 – 225.

[20] W. J. Evans, J. M. Perotti, S. A. Kozimor, T. M. Champagne, B. I. Davis, G. W. Nyce, C. H. Fujimoto, R. D. Clark, M. A. Johnston, J. W. Ziller, *Organometallics* **2005**, *24*, 3916 – 3931.

[21] For an irreversible insertion of [Me$_2$SiO] into a Yb−Me$_2$pz bond, see X. Zhou, H. Ma, X. Huang, X. You, *J. Chem. Soc. Chem. Commun.* **1995**, 2483 – 2484.

[22] a) For a reversible CO_2 insertion into a Sm−EPh bond (E = S, Se), see W. J. Evans, K. A. Miller, J. W. Ziller, *Inorg. Chem.* **2006**, *45*, 424 – 429; b) a scandium(III)-bonded β-diketiminato ("nannac")ligand framework was shown to reversibly capture CO_2: Ref. [14b].

[23] D. Werner, G. B. Deacon, P. C. Junk, R. Anwander, *Eur. J. Inorg. Chem.* **2017**, 3419 – 3428.

[24] H. C. Aspinall, J. Bacsa, A. C. Jones, J. S. Wrench, K. Black, P. R. Chalker, P. J. King, P. Marshall, M. Werner, H. O. Davies, et al., *Inorg. Chem.* **2011**, *50*, 11644 – 11652.

[25] J. A. Bogart, A. J. Lewis, S. A. Medling, N. A. Piro, P. J. Carroll, C. H. Booth, E. J. Schelter, *Inorg. Chem.* **2013**, *52*, 11600 – 11607.

[26] M. Begtrup, J. Elguero, R. Faure, P. Camps, C. Estopá, D. Ilavský, A. Fruchier, C. Marzin, J. de Mendoza, *Magn. Reson. Chem.* **1988**, *26*, 134 – 151.

[27] D. Werner, G. B. Deacon, P. C. Junk, R. Anwander, *Dalton Trans.* **2017**, *46*, 6265 – 6277.

[28] D. Werner, U. Bayer, N. E. Rad, P. C. Junk, G. B. Deacon, R. Anwander, *Dalton Trans.* **2018**, *47*, 5952 – 5955.

[29] U. Baisch, D. B. Dell'Amico, F. Calderazzo, L. Labella, F. Marchetti, D. Vitali, *J. Mol. Catal.* **2003**, *204 – 205*, 259 – 265.

[30] S. Bachmann, B. Gernert, D. Stalke, *Chem. Commun.* **2016**, *52*, 12861 – 12864.

[31] M. H. Chisholm, J. C. Gallucci, K. Phomphrai, *Inorg. Chem.* **2004**, *43*, 6717 – 6725.

[32] W. Clegg, R. W. Harrington, M. North, R. Pasquale, *Chem. Eur. J.* **2010**, *16*, 6828 – 6843.

[33] a) D. J. Darensbourg, M. W. Holtcamp, *Coord. Chem. Rev.* **1996**, *153*, 155 – 174; b) H. Jing, T. Chang, L. Jin, M. Wu, W. Qiu, *Catal. Commun.* **2007**, *8*, 1630 – 1634; c) J. Meléndez, M. North, R. Pasquale, *Eur. J. Inorg. Chem.* **2007**, 3323 – 3326; d) F. Jutz, J.-D. Grunwaldt, A. Baiker, *J. Mol. Catal. A* **2008**, *279*, 94 – 103; e) F. Jutz, J.-D. Grunwaldt, A. Baiker, *J. Mol. Catal. A* **2009**, *297*, 63 – 72; f) M. North, R. Pasquale, *Angew. Chem. Int. Ed.* **2009**, *48*, 2946 – 2948; *Angew. Chem.* **2009**, *121*, 2990 – 2992.

[34] Y. Liang, R. Anwander, *Dalton Trans.* **2013**, *42*, 12521 – 12545.

[35] For Ce^{IV} carboxylate MOFs, see a) P. Ji, T. Sawano, Z. Lin, A. Urban, D. Bours, W. Lin, *J. Am. Chem. Soc.* **2016**, *138*, 14860 – 14863; b) X.-P. Wu, L. Gagliardi, D. G. Truhlar, *J. Am. Chem. Soc.* **2018**, *140*, 7904 – 7912.

[36] For examples of dipyrazolyl-based MOFs, see a) H. J. Choi, M. Dinca, J. R. Long, *J. Am. Chem. Soc.* **2008**, *130*, 7848 – 7850; b) M. Tonigold, Y. Lu, B. Bredenkötter, B. Rieger, S. Bahnmüller, J. Hitzbleck, G. Langstein, D. Volkmer, *Angew. Chem. Int. Ed.* **2009**, *48*, 7546 – 7550; *Angew. Chem.* **2009**, *121*, 7682 – 7687; c) N. M. Padial, E. Q. Procopio, C. Montoro, E. López, J. E. Oltra, V. Colombo, A. Maspero, N. Masciocchi, S. Galli, I. Senkovska, S. Kaskel, E. Barea, J. A. R. Navarro, *Angew. Chem. Int. Ed.* **2013**, *52*, 8290 – 8294; *Angew. Chem.* **2013**, *125*, 8448 – 8452; d) Z. R. Herm, B. M. Wiers, J. A. Mason, M. R. Hudson, P. Zajdel, C. M. Brown, N. Masciocchi, R. Krishna, J. R. Long, *Science* **2013**, *340*, 960 – 964; e) J. A. Mason, J. Oktawiec, M. K. Taylor, M. R. Hudson, J. Rodriguez, J. E. Bachman, M. I. Gonazalez, A. Cervellino, A. Guagliardi, C. M. Brown, P. L. Llewellyn, N. Masciocchi, J. R. Long, *Nature* **2015**, *527*, 357 – 363.